Low-Density Hypersonic Flow over a Cone

R. HOFLAND* AND H. S. GLICK†
Rensselaer Polytechnic Institute, Troy, N.Y.

An experimental study of low-density hypersonic flow over a slender cone has been conducted using air and helium as the test gases. The test flows spanned a range of freestream Mach numbers from 12 to 24 in air, and from 36 to 80 in helium; the range of Reynolds numbers extended from 200 to 100,000. Pressures were monitored using miniature acceleration-compensated transducers. The experimental pressure data obtained at relatively high-density conditions are compared with the predictions of weak viscous-interaction theories, and the agreement is shown to be satisfactory if flow angularity, nozzle-flow gradients, and nonequilibrium effects are taken into account. In the intermediate range of flow densities, the recent viscous-interaction theory of Mirels and Ellinwood is found to have a limited domain of applicability due to the appearance of rarefaction effects. At the lowest density conditions studied experimentally, the flowfield in the vicinity of the vertex of the cone is believed to be outside the domain of existing continuum theories. However, an approximate calculation which takes into account the structure of the shock wave appears to give results which are in satisfactory agreement with the experimental data.

Introduction

THE problem of hypersonic viscous interaction has been studied extensively over the past fifteen years and a good measure of success has been achieved in understanding some of the main aspects of the problem.[1] To a large extent, the viscous-interaction problem is well understood for two-dimensional and slender axisymmetric bodies within the limits of boundary-layer theory based on the Navier-Stokes equations. As the flow is made progressively more rarefied, new phenomena are observed which modify the predictions of viscous-interaction theory. For example, it has been shown by many investigators that pressures measured on two-dimensional and slender axisymmetric bodies fall substantially below the values predicted by strong-interaction theory as the degree of rarefaction is increased.[2–4] Many theoretical efforts have been made to account for the departures from strong-interaction theory and some success has been achieved, especially for the case of the flat plate.[5–7]

The experimental studies of hypersonic viscous interaction have provided both a proving ground and a source of physical models for the theorist, especially for cases in which rarefaction effects are significant. The prime responsibility of the experimentalist has been to obtain data which are not spurious. This aim is not easily achieved because favorable signal-to-noise ratios are difficult to obtain at the low signal levels characteristic of rarefied hypersonic flow, pressure-orifice corrections become important, and extreme care must be exercised, especially for flat plates, to correct for flow angularity, three-dimensional flow effects, flow gradients, nose bluntness, etc. These experimental difficulties have produced marked disagreements in the data obtained in different experimental studies, and therefore comparisons with the predictions of various theories have not been unequivocal.

The present study has been carried out in a shock tunnel using air and helium as test gases. Data have been taken over a fairly wide range of densities so that the measurements extend from the weak-interaction regime up to relatively high degrees of rarefaction. The main aim of the present study has been to obtain data which will provide a meaningful test of theories which seek to describe phenomena involving rarefaction effects.

Experimental Apparatus

A. Shock Tunnel Configuration

The present experiments were carried out in a combustion-driven shock tunnel. A detailed description of the shock tunnel configuration, the auxiliary equipment, and the method of operation is given in Ref. 8.

B. Model and Instrumentation

The model employed in the experimental study is a pointed right-circular cone with a 10° semivertex angle (Fig. 1) and consists of a brass body with a detachable stainless steel tip. A hemispherically-headed impact-pressure probe (1.125 in. in diameter) is mounted 3.5 in. off the axis of the cone to provide continuous monitoring of the impact pressure in the test section. The nose of the probe (shown disassembled in Fig. 1) is located in the same transverse plane as that of the tip of the cone. A four-in.-long brass cylindrical afterbody is screwed into the rear of the cone and contains the field-effect-transistor (FET) amplifiers. A steel rod (1.25 in. in diameter and six ft long) screws into the back of the cylindrical afterbody, connecting the cone and the impact-pressure probe with the model-support mechanism which is capable of approximately six feet of translation along the axis of the tunnel.

The tip diameter of the nose has been chosen to be sufficiently small to obviate the complicating effects of bluntness interaction. If one applies the criterion developed by H. K. Cheng[9] for the case of a blunted flat plate to the case of a

Received December 5, 1968; revision received July 25, 1969. This work was sponsored both by the Aerospace Research Laboratories, Office of Aerospace Research, U. S. Air Force under Contract Number AF 33(615)-1080 and by NASA through a NASA Traineeship. The authors gratefully acknowledge the assistance provided by W. G. Burwell and V. J. Sarli of the United Aircraft Research Laboratories in the calculations of air test-section properties; the authors are indebted to J. W. Ellinwood of the Aerospace Corporation for discovering an error in one of the equations contained in the Appendix.

* Research Assistant; presently a member of the Technical Staff at the Aerospace Corporation, El Segundo, Calif. Member AIAA.

† Associate Professor of Aeronautical Engineering and Director of Hypersonic Research; presently Professor of Fluid Mechanics, University of Denver, Denver, Colo. Member AIAA.

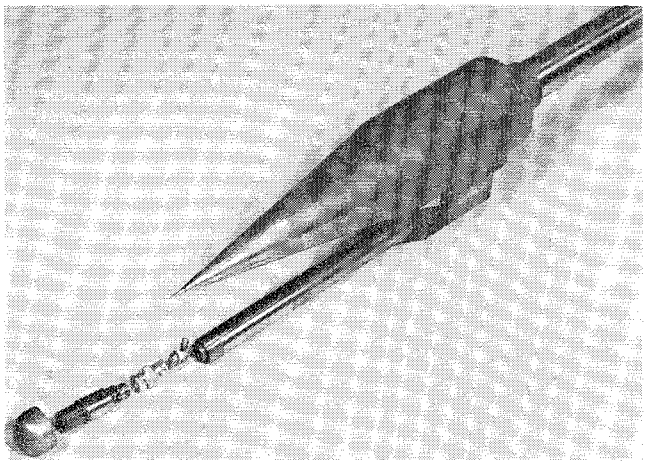

Fig. 1 Pressure-instrumented 10° cone and associated impact-pressure probe.

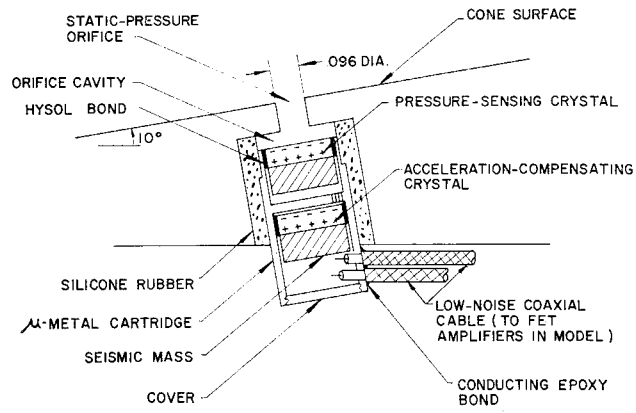

Fig. 2 Section view of an acceleration-compensated pressure transducer mounted in a 10° cone.

blunted cone, it is found that the condition for which nose-bluntness effects are negligible compared with viscous-interaction effects is

$$x/t \gg (Re_{\infty,t}/C_\infty M_\infty^2)(k/\epsilon)(0.664 + 1.73T_w/T_0)^{-2}$$

where t is the nose-tip diameter, k is the nose-drag coefficient, and $\epsilon = (\gamma - 1)/(\gamma + 1)$. This criterion is similar to that given in Ref. 1. It is readily determined that for the range of Reynolds numbers and Mach numbers employed in the present study, the aforementioned criterion implies that nose-bluntness effects are negligible. For the lowest Reynolds number experiments, it is not clear that this criterion remains meaningful since the requirements of continuum hypersonic slender-body theory are not satisfied. However, mean-free-path arguments can be developed which indicate that bluntness interaction is also unimportant in the highly rarefied flow experiments.[8]

The cone model has static pressure orifices at locations (based on slant distance along the surface) of 0.50, 2.20, 3.89, and 5.83 in. from the vertex. Each of the three downstream pressure transducers is located at the bottom of an orifice that is 0.096 in. in diameter and 0.100 in. in depth (Fig. 2), whereas the leading pressure transducer is located at the bottom of an L-shaped orifice that is 0.070 in. in diameter and 0.250 in. in total depth.

Reference 10 provides a detailed description of the fabrication and calibration of miniature acceleration-compensated pressure transducers employed in the present investigation. Particular attention is given to the problem of obtaining pairs of crystals whose acceleration response is similar over a wide frequency range. Also, the several important advantages of insulated-gate FET amplifiers, both in regard to transducer miniaturization and superior electronic performance, are described.

Reservoir, impact, and cone-surface-pressure records are presented in Fig. 3 for the most highly rarefied flow studied.

C. Flowfield Calibration

Flow uniformity in the contoured-nozzle test section was determined using aerodynamic probes. The distribution of impact pressure in the test section and measurements of the flow angularity along the test-section axis of symmetry were obtained for each test gas and reservoir condition of interest.

An impact-pressure rake was moved along the nozzle axis at three-in. increments and simultaneously monitored the transverse variation of impact pressure along a diametral line at either three- or four-in. increments. High-quality impact-pressure data have been obtained with little or no acceleration sensitivity (as determined by control tests with the orifices sealed). The axial Mach number gradient in air for the three nozzles studied is found to be approximately $\frac{1}{2}$ of 1% per in., where the Mach number is determined by computing the nonequilibrium expansion from the reservoir to the measured impact pressure. Inferred values of flow Mach number are believed to be accurate to within ±1%, the main contribution to the experimental error arising from a ±3% uncertainty in the pressure transducer sensitivities. The axial Mach number gradient in helium at nominal flow Mach numbers of 36 and 72 is approximately twice as high as for the airflows, or about 1% per in.

Typical radial distributions of impact pressure in the three contoured nozzles employed in the air experiments are shown in Fig. 4 for nominal test-section Mach numbers of 12, 18, and 24. The radial Mach number gradient, as computed from the measured impact-pressure surveys, is found to lie in the range 0.25 to 0.4% per in., where the Mach number in

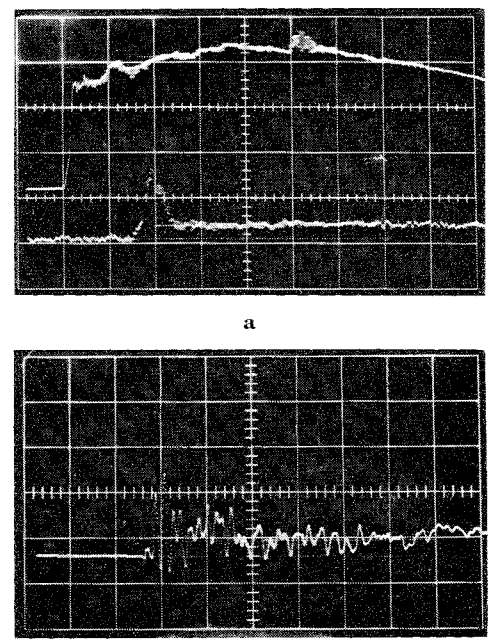

a

b

Fig. 3 Pressure records obtained in an airflow at M_∞ = 22.6, p_0 = 104 atm, T_0 = 3900 °K, Re_∞/in. = 400. a) The upper trace shows the reservoir pressure (500 psi/division); the lower trace shows the impact pressure (0.068 psi/division). The sweep speed is 500 μsec/division. b) The trace shows the output of an acceleration-compensated gauge mounted near the vertex of a 10° cone. The vertical sensitivity is 0.0028 psi/division and the sweep speed is 500 μsec/division.

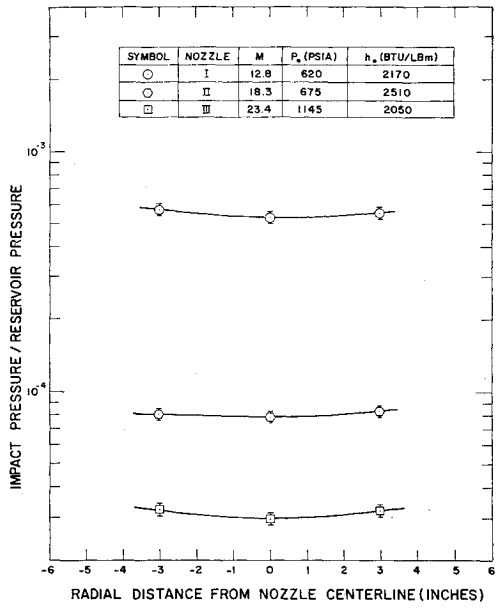

Fig. 4 Typical radial distributions of impact pressure in contoured hypersonic nozzles.

general falls with increasing radial distance from the nozzle centerline. The measured axial and radial gradients are almost independent of reservoir density.

The measurement of flow angularity along the test-section axis of symmetry for each test gas and reservoir condition of interest completed the nozzle-flow calibration. The pressure-instrumented 10° cone was used for this purpose.[8]

Results and Discussion

A. Data and Data Reduction Methods

An accurate determination of the hypersonic air and helium test-flow properties involves a number of special considerations. Included in these are the determination of time-dependent reservoir conditions, proper interpretation of measured impact pressures, and a consideration of thermodynamic nonequilibrium in the nozzle-expansion process.

Some care is also required to insure a proper interpretation and comparison of experimentally measured orifice pressures with theoretical surface-pressure predictions, since the latter have been obtained assuming a uniform freestream flow with no angle of incidence, and calorically and thermally perfect gas behavior.

1. Reservoir conditions

In order to obtain relatively long testing times with nearly constant reservoir properties, the combustion-driven shock tunnel was operated as close to the "tailored-interface" condition as possible. Reservoir temperatures are thereby restricted to the range 3400° to 3800°K for air, and 1200° to 1400°K for helium. However, it has not been possible, using the present shock tunnel, to achieve truly constant reservoir properties for either the air or the helium experiments. This difficulty is believed to be due to the excessive length-to-diameter ratio of the driven tube which is responsible for appreciable attenuation of the incident shock wave.

Reservoir properties were determined from 1) the measured speed of the incident shock wave just prior to reflection, 2) the measured reservoir pressure, and 3) the assumption that the gas in the reservoir is in thermodynamic equilibrium.[11] It can be shown from previously measured vibrational and chemical rate processes for atmospheric gases that the shock-heated air in the reservoir approaches thermochemical equilibrium in times that are negligible compared with tunnel-testing times. At 3600°K and 100 atm, the energy loss produced by radiation and conduction from the almost stagnant air to the cold shock-tube walls in five milliseconds is less than 4% of the total energy, and has therefore been ignored in the data reduction.

The reservoir pressure, calculated on the basis of the measured shock-wave speed and the initial pressure in the driven tube, is found to agree with the measured pressure just after shock reflection to within one or two per cent. The relatively small deviations of the reservoir gas properties from ideal tailored-interface conditions during a test are assumed to be caused by isentropic wave processes, and are accounted for accordingly.

2. Test-section properties

a) Air: During the rapid expansion of high-enthalpy air in the shock tunnel nozzle, departures from equilibrium flow conditions may occur. These nonequilibrium effects, caused by lags in energy transfer associated with chemical reactions and vibrational deactivation, may cause significant changes in test-section properties from values computed on the basis of an equilibrium expansion. Nonequilibrium effects are important enough in the present investigation so that detailed numerical computations were carried out for each nozzle geometry and nominal reservoir condition of interest.

An empirical equation, which was developed by Burke and Bird,[12] has been employed in estimating the boundary-layer correction necessary for specifying the effective inviscid boundary coordinates for each of the three nozzles of interest. The air kinetic model and the reaction rates used in the present calculations are given in Ref. 8. Test-section properties are determined by conducting the nonequilibrium computation from the reservoir to the measured impact pressure. After introducing small corrections for the effects of rarefaction, the measured impact pressure, p_0', is related to computed nonequilibrium flow properties by the relation

$$p_0' = \rho_{\infty n} U_{\infty n}^2 [1 - \tfrac{1}{2}(\rho_\infty/\rho_2)_e + O(M_\infty^{-2})]$$

where $(\rho_\infty/\rho_2)_e$ is the equilibrium density ratio across the normal bow shock in front of the impact probe, and the subscripts n and e refer to nonequilibrium and equilibrium values, respectively. Vibrational and rotational relaxation during the air expansion in the contoured nozzle has been studied in detail and is found to have a negligible influence in changing freestream properties from those values computed on the basis of instantaneous rotational and vibrational equilibration.[8] The predictions of nonequilibrium nozzle flow calculations, using models and reaction rates differing only slightly from the present scheme, have been found by a number of investigators to be in excellent agreement with experiment,[13,14] thus placing some confidence in the present technique for finding freestream flow conditions.

b) Helium: Helium is a monatomic gas that has been used for many years in steady-flow hypersonic studies. At reservoir temperatures on the order of a thousand degrees Kelvin, the fraction of helium atoms in excited electronic states is easily shown to be negligible. The extremely low condensation temperature of helium permits the expansion of helium from relatively low reservoir temperatures of 1200° to 1300°K up to flow Mach numbers of 80. Since these reservoir temperatures are small compared with the reservoir temperatures employed in the air experiments, the helium studies have large values of T_w/T_0 relative to the air studies.

It is shown in Ref. 8 that even for expansions up to Mach 80, helium behaves as a gas that is ideal, both thermally and calorically, and that the error in using the isentropic relations is less than 0.2%.

3. *Low-density corrections to measured pressures*

The problem of relating the measured orifice pressure to the surface pressure under rarefied flow conditions has been considered by Potter et al.[15] and Vidal and Bartz.[16] In these studies, an empirical result of Knudsen has been extended approximately by the methods of kinetic theory. For the range of interest in the present investigation, the predictions of the two theories are essentially indistinguishable. The orifice pressure, p_w, and the surface pressure, p_s, have been related by the following transcendental equation:

$$(p_s/p_w)^{2K} - \tfrac{15}{8}(\pi/2)^{1/2}K_w(p_s/p_w)^{K-1} - 1 = 0$$

where

$$K_w = \left(\frac{\gamma - 1}{\gamma}\right)^{1/2} \frac{Pr\dot{q}_w}{(C_pT_w)^{1/2}} \frac{1}{p_w}$$

$$K = \left[1 + 1.23\,\frac{d}{\lambda_w}\left(\frac{1 + 1.58d/\lambda_w}{1 + 12.25\,d/\lambda_w}\right)\right]$$

and λ_w/d is the orifice Knudsen number based on the orifice diameter and the measured orifice pressure, γ is the specific heat ratio, Pr is the Prandtl number, $\dot{q}_w$ is the heat-transfer rate at the wall, C_p is the specific heat at constant pressure, and T_w is the wall temperature. These relations follow from Ref. 16 after some rearrangement.

Based on these approximate analyses, corrections to the measured pressures due to "pseudo-thermal transpiration" were generally small in the present work, except for the case of the Mach 24 airflow, where corrections to the pressures measured one-half in. downstream of the cone vertex exceed 100%. The recent experimental work by Vidal and Bartz,[16] in which both flush-mounted and recessed transducers were employed in monitoring pressures in low-density hypersonic flows, suggests that the correction used here may underestimate the surface pressure by 10% to 20%. However, the kinetic pressure measured by the CAL flush-mounted transducer may have exceeded the predicted thermodynamic pressure because of rotational nonequilibrium. Until this question is resolved, the uncertainty in the pressure-orifice correction will continue to be the major source of error for the most highly rarefied flow experiments. At the higher density conditions where the pressure-orifice correction is small or negligible, the major source of error in the experiments arises from a ±3% uncertainty in the sensitivities of the pressure transducers.

Small viscous corrections to the measured impact pressure have also been made at the low-density flow conditions.[17]

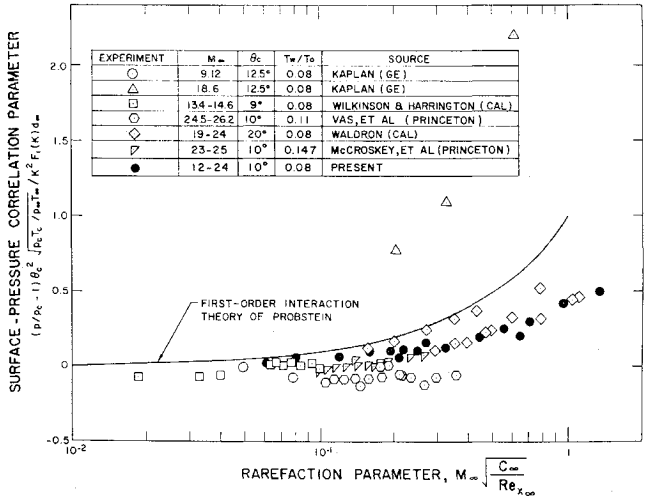

Fig. 5 Pressure distributions over pointed cones in hypersonic flows for cold-wall conditions. K is the hypersonic similarity parameter; $F_1(K,\gamma)$ and d_∞ (T_w/T_0, γ, M_∞, Pr) are defined in Ref. 18.

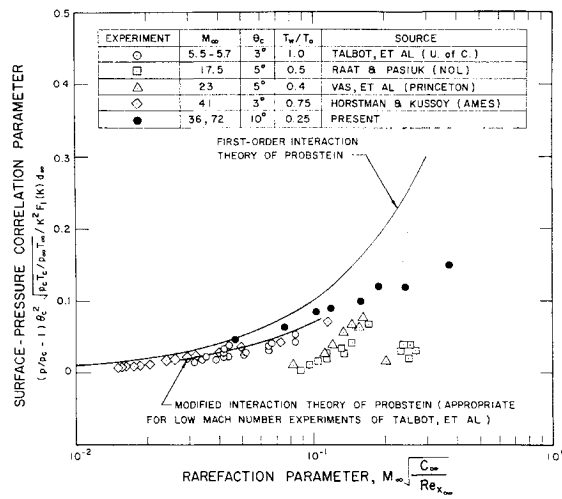

Fig. 6 Pressure distributions over pointed cones in hypersonic flows for hot-wall conditions. K is the hypersonic similarity parameter; $F_1(K,\gamma)$ and d_∞ (T_w/T_0, γ, M_∞, Pr) are defined in Ref. 18.

These corrections to the measured impact pressure have in no case exceeded 3%.

4. *Flow incidence*

Since nozzle flow angularity was found to vary with reservoir conditions and nozzle area ratio, slight misalignment of a slender cone in a shock-tunnel flow is difficult to avoid and may produce large asymmetry in the pressure distribution at high flow Mach numbers. For an inviscid hypersonic flow over a slender cone with a strong shock, the tangent-cone approximation gives the windward surface pressure with small pitch, α, in terms of the Taylor-Maccoll pressure, p_c, as

$$p(\alpha) = p_c(1 + \alpha/\theta_c)^2,\ (M_\infty\theta_c)^2 \gg 1$$

A one-degree flow misalignment is seen to cause a 21% increase in windward surface pressure for a 10° half-angle cone, whereas for more slender cones the alignment problem is considerably more severe. A method has been devised for reducing these errors by an order of magnitude or more, as discussed below.

For the case of a viscous flow over a cone at small incidence, the surface pressure, normalized with respect to the zero-incidence pressure, may be written in terms of a double power series expansion in α/θ_c and β/θ_c as follows:

$$\frac{p(x,\theta_c,\phi;\alpha,\beta)}{p(x,\theta_c)} = \sum_{m=0}\sum_{n=0}\left(\frac{\alpha}{\theta_c}\right)^m\left(\frac{\beta}{\theta_c}\right)^n p_{mn}(x,\theta_c,\phi)$$

where β is the yaw angle, $p_{00} = 1$, and $p_{mn} \leq 0(1)$. By symmetry considerations, one finds that p_{01} and p_{10} are odd functions of ϕ about π, and consequently,

$$p(x,\theta_c) = \frac{1}{4}\sum_{k=0}^{3} p(x,\theta_c,\phi + \frac{k\pi}{2};\alpha,\beta)\left[1 + O\left(\frac{\delta}{\theta_c}\right)^2\right]$$

where δ is the larger of the pitch and yaw angles. Hence, by making four separate measurements in which the cone is carefully rotated by increments of 90°, it is possible to infer the zero-incidence pressure distribution from distributions including small angles of pitch and yaw, with an error of order $(\delta/\theta_c)^2$ at most. In the present measurements, δ is estimated to vary between one-half to one degree, and $\theta_c = 10°$.

B. Experimental Results and Discussion

The present experimental results, as well as those obtained previously, are compared with the first-order weak-interaction theory of Probstein[18] in Figs. 5 and 6. The Probstein

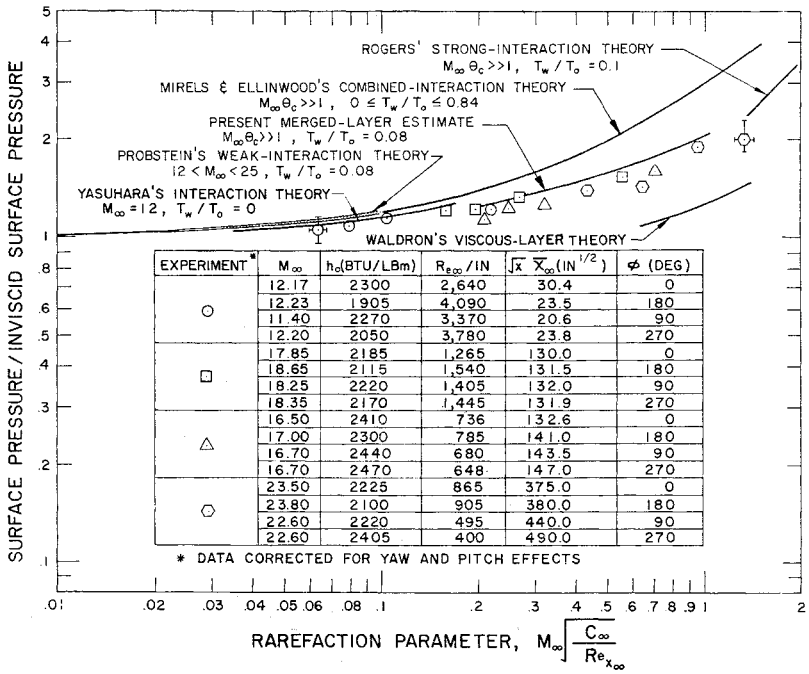

EXPERIMENT*	M_∞	h_o(BTU/LBm)	Re_∞/IN	$\sqrt{x}\,\bar{x}_\infty$(IN$^{1/2}$)	ϕ (DEG)
○	12.17	2300	2,640	30.4	0
	12.23	1905	4,090	23.5	180
	11.40	2270	3,370	20.6	90
	12.20	2050	3,780	23.8	270
□	17.85	2185	1,265	130.0	0
	18.65	2115	1,540	131.5	180
	18.25	2220	1,405	132.0	90
	18.35	2170	1,445	131.9	270
△	16.50	2410	736	132.6	0
	17.00	2300	785	141.0	180
	16.70	2440	680	143.5	90
	16.70	2470	648	147.0	270
⬡	23.50	2225	865	375.0	0
	23.80	2100	905	380.0	180
	22.60	2220	495	440.0	90
	22.60	2405	400	490.0	270

Fig. 7 The present air data compared with various theoretical analyses.

theory has been used in these figures because it permits a convenient comparison of data obtained under differing flow conditions. It will be shown later that the curves given by the Probstein theory are almost indistinguishable from those predicted by the later analyses of Yasuhara[19] and Mirels and Ellinwood.[20] Indeed, it can be shown that Probsetin's first-order theory is satisfactory for correlating data both in the weak and in the moderate interaction regimes in the absence of rarefaction effects. Figure 5 shows how the various data correlate for the case of a cold wall. It is seen that the present results are the only set of data which clearly merges with the Probstein curve at small values of the rarefaction parameter, i.e., $\bar{V}_\infty \le 0.10$, and departs from the theoretical curve as $\bar{V}_\infty$ increases. The data of Waldron[4] suggest a similar behavior, but apparently there are two sets of results—one set which follows the theoretical curve closely up to values of $\bar{V}_\infty$ of approximately 0.35 and then falls below, and a second set which is roughly parallel with the first set, but lies somewhat below it. Although spanning a somewhat larger range of conditions, the present data are largely bracketed by the composite results of Waldron. Also, the present results are reasonably close to those obtained by McCroskey et al.[21] over the range $0.09 \le \bar{V}_\infty \le 0.27$. However, the data of McCroskey et al. do not quite merge with the Probstein curve at values of $\bar{V}_\infty \le 0.10$. The differences between the present data and those of Waldron and McCroskey et al. are not large, and can probably be attributed to the difficulties inherent in low-density hypersonic flow measurements. The data of Kaplan,[22] Wilkinson and Harrington,[23] and Vas et al.[24] are noticeably different from the previously discussed data, and the reasons for the lack of correlation between these latter data and the Probstein curve are not known.

The various experimental results for the hot-wall case are shown in Fig. 6. The present data are again seen to merge with the Probstein curve at values of $\bar{V}_\infty \cong 0.10$ and fall below the theoretical curve as the value of $\bar{V}_\infty$ is increased. The relatively low Mach number results of Talbot et al.[25] apparently follow the Probstein theory (modified for low-flow Mach numbers) up to values of $\bar{V}_\infty \cong 0.085$, with no appreciable indication of rarefaction effects. The recent data of Horstman and Kussoy[26] lie slightly below the present results up to values of $\bar{V}_\infty \cong 0.10$, and are also slightly below the Probstein curve at low values of $\bar{V}_\infty$, i.e., $\bar{V}_\infty \le 0.05$. Considering the small differences between the present results and those of Horstman and Kussoy, and the slow rate of departure of these data from the theoretical curve, it is not clear that the apparent earlier departure of the data of Horstman and Kussoy from the theoretical curve is quantitatively significant even though an earlier departure would be expected on theoretical grounds. The results of Vas et al.[24] and Raat and Pasiuk[27] are noticeably different from the present data, both qualitatively and quantitatively. The reasons for these appreciable differences are not known.

In order to facilitate an understanding of the departure of the experimental data from viscous-interaction theory, an exploratory analysis was carried out for the merged-layer flow over a cone. The goal of this analysis is to explain by approximate methods the observed reductions in measured pressure below viscous-interaction predictions on the basis of a continuum-flow model which provides a connection between the kinetic or noncontinuum flow upstream and the hypersonic viscous-interaction flow downstream. In view of some recent work in which the flowfield near the vertex of a sharp cone has been probed,[21] it was anticipated that the shock structure will be merged with that of the viscous layer, and that the shock wave and the processes which take place in it should be expected to assume major importance.

A modified version of the Rankine-Hugoniot equations was developed in Ref. 8 by integrating a simplified form of the Navier-Stokes equations across the shock-transition zone, and the resulting conical shock solution was patched to the combined-interaction boundary-layer solution of Mirels and Ellinwood,[20] where the latter solution is only valid when rarefaction effects are negligible (see Appendix I). The modified conical shock-jump conditions account for transport processes immediately behind the compression zone, but shock curvature and thickness effects are assumed to be of higher order in this formulation. The conical shock zone is patched to the viscous layer zone by requiring continuity in normal velocity and normal velocity gradient at the shock-viscous-layer interface. A discontinuity in tangential velocity and total enthalpy at the interface is implicit in the patching procedure, but these discontinuities are believed to cause only small errors in the physical flow properties.

In Fig. 7, the present experimental data are compared with the approximate theoretical analysis described previously, as well as with other theoretical treatments. This figure shows how the cone pressure varies as a function of the rarefaction parameter, $\bar{V}_\infty$, over a range extending from the weak-inter-

action domain up to the noncontinuum region. As mentioned earlier, the results obtained from the first-order theory of Probstein are seen to be quite close to those predicted by the theories of Yasuhara and Mirels and Ellinwood.

Figure 7 also shows the theoretical curves obtained from the studies of Waldron[4] and Rogers.[28] The analysis of Rogers is based on a strong-interaction model in which transverse curvature is assumed to be small. It may be shown that such an analysis is conceptually wrong since a strong-interaction model implies large transverse curvature.[8] The curve of Rogers shown in Fig. 7 is his zeroth-order solution, i.e., no transverse curvature, and it is seen that the curve of Mirels and Ellinwood appears to be in reasonable agreement with the Rogers' curve at large values of $\bar{V}_\infty$, indicating that the effect of transverse curvature on the rate of boundary-layer growth, and therefore on the pressure distribution, is small. The viscous-layer theory of Waldron lies appreciably below the present experimental data at values of $\bar{V}_\infty \cong 1$, but the slope of the curve is close to that given by the experimental data.

The results of the present approximate analysis for the pressure at the surface of the cone are compared with the experimental data in Fig. 7. The pressure prediction is seen to fall increasingly below that of Ref. 20 with increasing degrees of rarefaction, in satisfactory agreement with the low-density data, and reduces to the prediction of Ref. 20 for small degrees of rarefaction. The agreement between the experimental data and the approximate analysis appears to be somewhat better in the air experiments (cold-wall case) than in the helium tests (hot-wall case). In order to compare the air and helium tests, the data were correlated using the first-order Probstein analysis, and this data correlation is shown in Fig. 8. Also, the two curves obtained from the present approximate analysis are shown. The two sets of data appear to correlate better than the two approximate theoretical curves, although the differences between the two curves are small.

In order to understand why the experimental data correlate so well, a study was made to estimate the importance of other rarefaction effects which were not included in the present analysis. The appearance of velocity slip and temperature jump at the interface between the cone and the flowing gas has been investigated using the criterion given in Ref. 20. It is found that these low-density effects are unimportant in the air experiments when $\bar{V}_\infty \leq 0.22$, and are negligible in the helium tests when $\bar{V}_\infty \leq 0.11$. The variation of pressure across the boundary layer due to increased streamline curvature and thickening of the viscous layer at low densities has been considered, where surface slip is included in an approximate fashion.[8] For $\bar{V}_\infty \leq 0.25$, the maximum fractional error made by neglecting normal pressure-gradient effects is found to be less than 2% for the air viscous layer and less than 8% for the helium viscous layer. In Fig. 8, it is seen that the air data tend to fall below the approximate theoretical curve at values of $\bar{V}_\infty \cong 0.3$, whereas the helium data appear to deviate at values of $\bar{V}_\infty \cong 0.2$. Although the scatter in the data and the approximate nature of the theoretical analysis do not permit unequivocal conclusions, it appears that merging effects and surface-slip effects are occurring at about the same values of $\bar{V}_\infty$, and that for the present experiments, the merging effects seem to be more important. It is expected that for more slender cones, especially for hot-wall conditions, the relative importance of shock-merging and boundary-layer rarefaction effects may be different.

Concluding Remarks

It is believed that the present study has provided accurate experimental data at hypersonic flow conditions where rarefaction effects produce significant deviations from continuum viscous-interaction predictions. An approximate analysis, which examines the merging of the conical shock wave with the viscous layer, appears to account fairly well for the observed behavior of the air and helium data over the whole experimental range. Some small deviations from this approximate theory are observed at the higher values of $\bar{V}_\infty$ where the experimentally-measured pressures fall somewhat below the theoretical curves. It appears likely that these deviations may be due to wall-rarefaction and normal-pressure-gradient effects, and possibly to differences between the normal stress and the thermodynamic pressure at the surface. In order to determine the validity of these speculations in a definitive manner, a comprehensive continuum analysis is needed which includes the phenomena of merging and boundary-layer rarefaction. On the basis of the present results, it appears likely that such an analysis may be accurate up to surprisingly high values of $\bar{V}_\infty$.

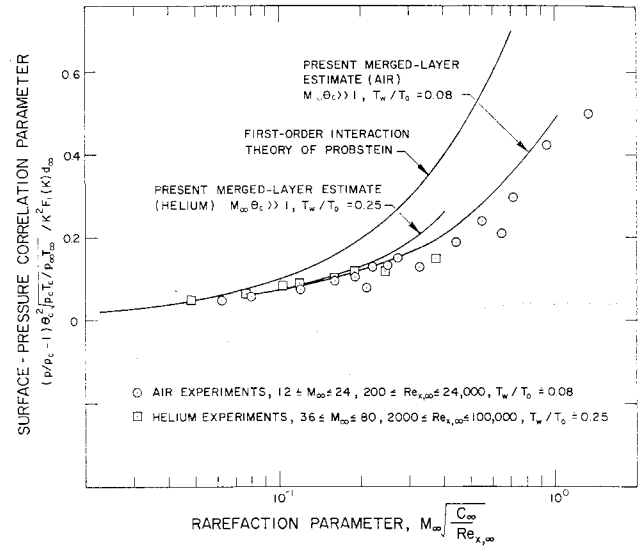

Fig. 8 Comparison of the present air and helium data with the present approximate merged-layer analysis and the first-order theory of Probstein. K is the hypersonic similarity parameter; $F_1(K,\gamma)$ and d_∞ (T_w/T_0, γ, M_∞, Pr) are defined in Ref. 18.

Appendix: Merged-Shock Analysis

An approximate analysis of the pressure distribution over a slender cone has been carried out for conditions under which the shock wave merges with the viscous layer. In the present treatment, the shock structure is determined using a simplified Navier-Stokes model since recent theoretical and experimental results indicate that the Navier-Stokes description of shock structure is fairly good in the downstream region, even in the case of strong shock waves.[29,30] The simplified shock structure is then patched to the combined-interaction viscous-layer solution of Mirels and Ellinwood.[20] The details of the present analysis are given in Ref. 8. In this Appendix, an outline of the method is presented and the main analytical result is given.

It may be shown that when terms of order δ_s/r_s and $\delta_s/R_L \tan^2\beta$ are small compared to unity in the Navier-Stokes equations (where δ_s is the shock thickness, r_s is the shock radius, R_L is the longitudinal radius of curvature of the shock, and β is the shock wave angle), the jump conditions across the conical shock may be expressed as

$$v_2' = (\rho_\infty/\rho_2)v_\infty' \tag{A1}$$

$$u_2' = u_\infty'[1 + (1/\rho_\infty U_\infty^2 \sin\beta \cos\beta)(\mu\, du'/dn)_2] \tag{A2}$$

$$p_2 = p_\infty + \rho_\infty v_\infty'^2(1 - v_2'/v_\infty') + (\tilde{\mu}\, dv'/dn)_2 \tag{A3}$$

$$H_2 = H_\infty \left(1 + \frac{2}{\rho_\infty U_\infty{}^3 \sin\beta} \left\{ \frac{\mu}{Pr} \frac{d}{dn} \left[H - (1 - Pr) \frac{u'^2}{2} - \frac{v'^2}{2} \left(1 - \frac{4}{3} Pr\right) \right] \right\}_2 \right) \quad \text{(A4)}$$

where μ is the coefficient of viscosity, $\tilde{\mu} = \frac{4}{3}\mu + K_B$, K_B is the bulk viscosity, and u' and v' are the velocity components in a left-handed orthogonal (s,n) coordinate system in which the coordinate s is taken to be the distance along the shock from the cone vertex and the coordinate n is taken to be the distance along one of the normals.

In order to patch the simplified shock structure solution to that of Mirels and Ellinwood, the velocities and velocity gradients are first transformed from curvilinear shock-oriented coordinates to body-oriented boundary-layer coordinates. If $\psi \equiv \beta - \theta_c$, then it can be shown

$$(\partial u'/\partial n)_2 \cong -\cos^2\psi (\partial u/\partial y)_2 \quad \text{(A5)}$$

and

$$u_2' \cong U_\infty \cos\beta [1 - (\cos^2\psi/\gamma M_\infty{}^2 \sin\beta \cos\beta)(\mu_2/p_\infty) \times (\partial u/\partial y)_2] \quad \text{(A6)}$$

Similarly, one can show that

$$(\partial v'/\partial n)_2 \cong -\sin\psi \cos\psi (\partial u/\partial y)_2 + \cos^2\psi (\partial v/\partial y)_2 \quad \text{(A7)}$$

and

$$v_2'/v_\infty' \cong (\cos\theta_c/\sin\beta) [\sin\psi - (v/u)_2 \cos\psi] \quad \text{(A8)}$$

It has been shown by Mirels and Ellinwood that the inviscid cone pressure, p_c, can be expressed as

$$p_c = p_\infty k^2 \gamma M_\infty{}^2 \theta_c{}^2 \quad \text{(A9)}$$

where k^2 is a weak function of the effective-body shape and the ratio of specific heats, and varies by a few percent over the weak-to-moderate interaction region. Combining Eqs. (A3), (A8), and (A9) yields

$$\frac{p_2}{p_c} \cong \frac{1}{\gamma(kM_\infty\theta_c)^2} + \frac{\sin^2\beta}{k^2\theta_c{}^2} \left[1 - \cos^2\theta_c \times \left(1 - \frac{\tan\theta_c}{\tan\beta}\right)\left(1 - \frac{(v/u)_2}{\tan\psi}\right) \right] + \frac{\tilde{\mu}_2/p_\infty}{\gamma(kM_\infty\theta_c)^2} \left(\frac{dv'}{dn}\right)_2 \quad \text{(A10)}$$

Using results given in Ref. 20, it can be shown that

$$(v/u)_2 \cong (\delta_1/2)(1 + 3.46 g_w)\ (\bar{V}_\infty/\theta_c) \cos^{1/2}\theta_c \quad \text{(A11)}$$

and

$$\tan\beta \cong (\tan\theta_c/\zeta_w)[1 + (\delta_1/2)(1 + 3.46 g_w)(\bar{V}_\infty/\theta_c{}^2) \times \cos^{1/2}\theta_c] \quad \text{(A12)}$$

where

$\delta^*(x)$ = displacement thickness = $\delta_1(1 + 3.46 g_w) \times x\bar{V}_\infty \cos^{1/2}\theta_c/\theta_c$

$\bar{V}_\infty(x)$ = local rarefaction parameter = $M_\infty(C_\infty\mu_\infty/\rho_\infty U_\infty x)^{1/2}$

$$g_w = 2C_pT_w/(2C_pT_\infty + U_\infty{}^2)$$

and ζ_w = radial location of edge of boundary-layer/radial location of shock.

In Eq. (A10), the value of $(dv'/dn)_2$ is obtained from Eq. (A7) by assuming that $(\partial u/\partial y)_2 \cong U_\infty/\delta^*$ and that $\cos\psi(\partial v/\partial y)_2 \ll \sin\psi(\partial u/\partial y)_2$. The former assumption can be justified for the case of hypersonic flow over slender bodies; the latter assumption is probably not uniformly valid throughout the inner viscous layer, although it can be shown to be accurate near the cone surface.

Using the preceding equations and assumptions, it can be shown that the pressure on the cone surface, p_e, is given by the relation

$$\frac{p_e}{p_c} \cong \frac{1}{\zeta_w k^2} \left\{ 1 + \left[\frac{\delta_1}{\theta_c{}^2} (1 + 3.46 g_w) - \frac{4}{3}\gamma \frac{(1 - \zeta_w)^2}{\zeta_w} \times \frac{\theta_c{}^2}{\delta_1(1 + 3.46 g_w)} \right] \bar{V}_\infty + \left[\frac{\delta_1{}^2}{4\theta_c{}^2} (1 + 3.46 g_w)^2 - \frac{2}{3}\gamma \times \frac{(1 - \zeta_w)}{\zeta_w} (3 - 2\zeta_w) + \frac{16}{9}\gamma^2 \frac{(1 - \zeta_w)^4}{\zeta_w{}^2} \frac{\theta_c{}^4}{\delta_1{}^2(1 + 3.46 g_w)^2} \right] \times \bar{V}_\infty{}^2 - \left[\frac{\gamma}{3} \frac{(1 - \zeta_w)(3 - \zeta_w)}{\zeta_w} \frac{\delta_1}{\theta_c{}^2} (1 + 3.46 g_w) - \frac{16}{9}\gamma^2 \frac{(1 - \zeta_w)^3(2 - \zeta_w)}{\zeta_w{}^2} \frac{\theta_c{}^2}{\delta_1(1 + 3.46 g_w)} + \frac{64}{27}\gamma^3 \frac{(1 - \zeta_w)^6}{\zeta_w{}^3} \frac{\theta_c{}^6}{\delta_1{}^3(1 + 3.46 g_w)^3} \right] \bar{V}_\infty{}^3 + O(\bar{V}_\infty{}^4) \right\}$$

for $\bar{V}_\infty \leq O(1)$ (A13)

where the pressure at the shock wave-viscous layer interface, given by Eq. (A10), has been replaced by the pressure at the surface of the cone with a maximum fractional error of the order of $(\delta_1\bar{V}_\infty/\theta_c)^2$, which may be ignored to the order of accuracy considered here.

References

[1] Hayes, W. D. and Probstein, R. F., *Hypersonic Flow Theory*, Academic Press, New York, 1959.

[2] McCroskey, W. J., Bogdonoff, S. M., and McDougall, J. G., "An Experimental Model for the Leading Edge of a Sharp Flat Plate in Rarefied Hypersonic Flow," *AIAA Journal*, Vol. 4, No. 9, Sept. 1966, pp. 1580–1587.

[3] Vidal, R. J. and Bartz, J. A., "Experimental Studies of Low-Density Effects in Hypersonic Wedge Flows," *Rarefied Gas Dynamics*, edited by J. de Leeuw, Vol. I, Academic Press, New York, 1965, pp. 467–486.

[4] Waldron, H. F., "Viscous Hypersonic Flow over Pointed Cones at Low Reynolds Number," *AIAA Journal*, Vol. 5, No. 2, Feb. 1967, pp. 208–218.

[5] Pan, Y. S. and Probstein, R. F., "Rarefied-Flow Transition at a Leading Edge," *Fundamental Phenomena in Hypersonic Flow*, edited by J. G. Hall, Cornell Univ. Press, 1966, pp. 259–306.

[6] Oguchi, H., "Shock Wave and Viscous Layer Structure in a Rarefied Hypersonic Flow Near the Leading Edge of a Sharp Flat Plate," Rept. 418, Univ. of Tokyo, Dec. 1967.

[7] Shorenstein, J. L. and Probstein, R. F., "The Hypersonic Leading Edge Problem," *AIAA Journal*, Vol. 6, No. 10, Oct. 1968, pp. 1898–1906.

[8] Hofland, R., "Studies in Rarefied Gasdynamics: I. Low-Density Hypersonic Flow Over a Cone, II. Scattering of Gas Particles from a Solid Surface," Ph. D. Thesis, Rensselaer Polytechnic Institute, Troy, N.Y., April 1969.

[9] Cheng, H. K., "Hypersonic Flow with Combined Leading-Edge Bluntness and Boundary-Layer Displacement Effect," Rept. AF-1285-A-4, Aug. 1960, Cornell Aeronautical Lab.

[10] Hofland, R. and Glick, H. S., "A Miniature Transducer for Measuring Low Transient Pressures," *The Review of Scientific Instruments*, Vol. 40, No. 9, Sept. 1969, pp. 1146–1151.

[11] Feldman, S., "Hypersonic Gas Dynamic Charts for Equilibrium Air," Avco Research Laboratory, Jan. 1957.

[12] Burke, A. F. and Bird, K. D., "The Use of Conical and Contoured Expansion Nozzles in Hypervelocity Facilities," Rept. 112, 1962, Cornell Aeronautical Lab.

[13] Duffy, R. E., "Experimental Study of Nonequilibrium Expanding Flows," *AIAA Journal*, Vol. 3, No. 2, Feb. 1965, pp. 237–244.

[14] Zonars, D., "Nonequilibrium Regime of Airflows in Contoured Nozzles: Theory and Experiments," *AIAA Journal*, Vol. 5, No. 1, Jan. 1967, pp. 57–63.

[15] Potter, J. L., Kinslow, M., and Boylan, D. E., "An Influence of the Orifice on Measured Pressures in Rarefied Flow," TDR-64-175, Sept. 1964, Arnold Engineering Development Center.

[16] Vidal, R. J. and Bartz, J. A., "Experimental Study of Pseudo Transpiration at an Orifice in Rarefied Flow," *Rarefied Gas Dynamics*, edited by L. Trilling and H. Y. Wachman, Vol. I, Academic Press, New York, 1969, pp. 639–653.

[17] Potter, J. L. and Bailey, A. B., "Pressures in the Stagnation Regions of Blunt Bodies in the Viscous-Layer to Merged-Layer Regimes of Rarefied Flow," TDR-168, Sept. 1963, Arnold Engineering Development Center.

[18] Probstein, R. F., "Interacting Hypersonic Laminar Boundary Layer Flow Over a Cone," Rept. No. AF2798/1, March 1955, Brown Univ.

[19] Yasuhara, M., "Axisymmetric Viscous Flow Past Very Slender Bodies of Revolution," *Journal of the Aerospace Sciences*, Vol. 29, June 1962, pp. 667–688.

[20] Mirels, H. and Ellinwood, J. W., "Hypersonic Viscous Interaction Theory for Slender Axisymmetric Bodies," *AIAA Journal*, Vol. 6, No. 11, Nov. 1968, pp. 2061–2070.

[21] McCroskey, W., Bogdonoff, S., and Genchi, A., "Leading Edge Flow Studies of Sharp Bodies in Rarefied Hypersonic Flow," *Rarefied Gas Dynamics*, edited by C. L. Brundin, Vol. II, Academic Press, New York, 1967, pp. 1047–1066.

[22] Kaplan, M., "Low Density Effects on Cone Pressure and Heat Transfer at Hypervelocity Speeds," TM-212, Nov. 1961, General Electric.

[23] Wilkinson, D. B. and Harrington, S. A., "Hypersonic Force, Pressure and Heat Transfer Investigations of Sharp and Blunt Slender Cones," TDR 73-117, Aug. 1963, Arnold Engineering Development Center.

[24] Vas, I., McDougall, J., Koppenwallner, G., and Bogdonoff, S. M., "Some Exploratory Experimental Studies of Hypersonic Low Density Effects on Flat Plates and Cones," *Rarefied Gas Dynamics*, edited by J. de Leeuw, Vol. I, Academic Press, New York, 1966, pp. 508–534.

[25] Talbot, L., Koga, T., and Sherman, P. M., "Hypersonic Viscous Flow Over Slender Cones," *Journal of the Aerospace Sciences*, Vol. 26, Nov. 1959, pp. 723–730.

[26] Horstman, C. C. and Kussoy, M. I., "Hypersonic Viscous Interaction on Slender Cones," *AIAA Journal*, Vol. 6, No. 12, Dec. 1968, pp. 2364–2371.

[27] Raat, J. and Pasiuk, L., "Rarefaction Effects in Hypersonic Boundary Layers," *AIAA Journal*, Vol. 4, No. 11, Nov. 1966, pp. 2052–2054.

[28] Rogers, D. F., "An Analytical Study of Hypersonic Viscous Flow Over an Unyawed Slender Cone at Moderately Low Densities," Ph.D. Thesis, Rensselaer Polytechnic Institute, Troy, N. Y., June 1967.

[29] Liepmann, H. W., Narasimha, R., and Chahine, M. T., "Structure of a Plane Shock Layer," *The Physics of Fluids*, Vol. 5, Nov. 1962, pp. 1313–1324.

[30] Camac, M., "Argon Shock Structure," *Rarefied Gas Dynamics*, edited by J. H. de Leeuw, Vol. I, Academic Press, New York, 1965, pp. 240–249.